Three-Dimensional Tetrahedron Network (3D TEN) and Volumetric Geo-Objects (VGO) Data Model for Groundwater Simulation in Bida Basin, Nigeria

Izham Mohamad Yusoff[1], Ishaku Bashir Yakubu[2]

[1]Geography Section, School of Distance Education, Universiti Sains Malaysia, 11800 USM Penang, Malaysia.
[2]Department of Geography, Faculty of Natural Sciences, Ibrahim Badamasi Babangida University, PMB 11, Lapai, Niger State, Nigeria.

Correspondence: Izham Mohamad Yusoff (email: izham@usm.my)

Received: 26 April 2022; Accepted: 1 September 2022; Published: 30 November 2022

Abstract

The presence of complex ground soil structures limits the attempt for groundwater extraction for alternate water supply usage. Hydrologists and engineers have made many attempts to Model 3D groundwater flow and storage using digital elevation model (DEM) data structures but have resulted in limited success in terms of actual 3D subsurface geology representation. This study attempts to construct resistivity data in an actual 3D environment using volumetric geo-objects (VGOs) and 3D tetrahedron network (3D TEN) data structures. Subsurface data were collected using the vertical electrical sounding (VES) approach to analyse the geological structure of the study area. To determine the course and movement of groundwater, the 3D constant was applied from Darcy's law in the Lagrangian technique. A time frame of one hour, two hours, four hours and eight-hour intervals was tested to simulate the porosity and permeability of various soil types with complex geological structures. The findings validated the use of 3D visualisation to model resistivity data. The implemented volumetric geo-object (VGO) data model and the 3D TEN model show the volume of water over the topsoil to be 17,461,228.07 in an hour; clay soil was 870,614.04; clayey sand was 435,307.02; and sandy clays was 348,245.61 per kilometre cube (km3). The use of 3D TEN and VGO for groundwater simulation in this research offers an improved perspective in groundwater visualisation that will promote sustainable groundwater exploration for societal developments. The findings of this study will be beneficial to stakeholders, water resource managers and government agencies such as Ministry of Water Resources.

Keywords: Data model, Groundwater simulation, Three-dimensional tetrahedron network (3D TEN), Vertical electrical sounding (VES), Visualisation, Volumetric geo-objects (VGOs)

Introduction

Groundwater extraction has become important due to the unpredictability of surface water sources. Many researchers and scholars, such as Omolaiye et al. (2020); Arowoogun and Osinowo (2022); and Gaikwad et al. (2022), have combined the geographical information system (GIS), remote sensing and vertical electrical sounding (VES) for groundwater prospecting with appealing results. The output of VES and GIS groundwater exploration models, on the other hand, are usually in two dimensions (2D), which has limited 3D representation of the subsurface that could provide more robust information that is critical to prospected well performances (Cedrick et al., 2021; Li et al., 2022). Furthermore, as the population grows, policy-makers require a model that can visualise 3D hydrogeological processes geared towards meeting the water supply needs for a growing populace.

The Transport of Unsaturated Groundwater and Heat (TOUGH 2) (Webb et al. 2018), Modular Three-Dimensional Finite-Difference Groundwater Flow Model (MODFLOW), (Langevin et al., 2017) and computer intelligence are examples of 3D modelling applications that can be used to investigate the groundwater yield potential of a specified region. Nonetheless, the current model ignores the characteristics of subsurface water flow, which includes geological material and permeability, in addition to a well-established structure of voids in distinct landforms (Omar et al., 2020).

Despite advances in computer graphics and the introduction of computers with high processing power, 3D GIS researchers have been unable to study various phenomena in 3D, such as static and dynamic fields, utilising various 3D GIS data processing models (Li et al., 2022; Zavari et al., 2022). The absence of an analytical model for subsurface water study and development has hampered the depiction of geological structures in 3D (Di Salvo et al., 2020). Gong et al. (2004) defined 3D GIS models as volume, surface and octree-based data models, allowing 3D GIS users to capture and visualise objects and events in 3D. Excessive line flow and pollutant distribution were assessed and visualised in 3D by researchers such as Izham et al. (2011), Zaidi et al. (2015), and Morosini and Zucaro (2019).

A key prerequisite for 3D groundwater modelling within geologic media is the knowledge and behaviour of the lithological units, as evident in the work of Di Salvo et al. (2020) and Zang (2022) using GoCAD in modelling strata, ores and faults. For GIS applications, Anh (2011) and Tuan (2013) provide a 3D GIS data model that includes 3D Format Data Structure (3D-FDS), 3D Tetrahedral Network (3D TEN), Object Oriented Model (OO 3D), 3D City Models (3D CityGML), Octree model, Simplify Spatial Model (SSM), Urban Data Model (UDM) and Solid Object Management System (SOMS) among many 3D GIS data models that are in practice today. Many of these 3D GIS models have found wide application in topology and smart urban city design with appealing results (Nasir et al., 2021). In terms of dynamic field visualisation as simulations, numerical, volumetric and other geo-objects have effectively been implemented in emergency planning, such as fire (Huang et al., 2019; Li et al., 2021), flood (Joy et al., 2020; Rydvanskiy & Hedley, 2020) and landslide modelling (Fanos et al., 2020; Havenith, 2021), using a volumetric data model with a unique speed and direction over time under different pressure conditions.

Therefore, this research uses the 3D Tetrahedron Network (TEN) and volumetric geo-object (VGO) data model to represent and visualise *in situ* data produced by VES into a 3D local visualisation of subsurface geological structures, specifying the issue of a specialised data structure compatible with 3D subsurface water simulation and modelling. The specific objectives of the research are to (i) identify and delineate the different lithological layers in the study area and (ii)

produce a 3D model delineated using the 3D TEN data model and simulate groundwater flow over the 3D modelled layers over time.

Literature review

Groundwater theory, simulation modelling techniques and tools

Groundwater hydrology is defined by part of the water from the stream, rainfall, and other recharge processes that have infiltrated the subsurface layer through the phreatic zone and confined to saturated voids and may be discharged into a well and seep over time. The subsurface layer water holding capacity is a function of porosity in water-bearing rock or soil voids defined by the ratio of water volume to the ratio of the lithological material void volume (Andriani et al., 2021; Akinyemi, 2022).

The volumetric water in the saturated media is a function of the unsaturated zone, which serves as an initiating change factor in the moisture content during saturation. The water content in the unsaturated zone changes over time and space and becomes saturated fluid phases of air and water. This phenomenon becomes more pronounced during the groundwater recharge process either from infiltration from precipitation or from nearby streams and rivers. The literature has demonstrated the assessment of groundwater retention capacity using a water retention capacity curve approach with a high success rate (Ekanem, 2020; Zeitoun et al., 2021), demonstrating the possibility of assessing water performance in subsurface media.

Therefore, in the process of simulating groundwater confined within geologic media, volumetric water content is critical. Lamontagne-Hallé et al. (2020) and Li et al. (2020) implemented a numerical modelling approach to simulate groundwater under different conditions. These studies offer a useful conceptual framework in groundwater simulation; however, this approach may result in variations from real conditions, and the results from such studies are often difficult to implement due to the imaginary parameter estimation (Ahmad et al., 2020; Luo et al., 2022). In overcoming this limitation, in 3D simulations, data models such as volumetric soft geo-objects (Izham et al., 2011; Maiti & Chakravarty, 2021), MODFLOW (Jaxa-Rozen et al., 2019; Xiang et al., 2020), and TOUGH 2 (Xu et al., 2021), among several other 3D data models, have been used in the simulation of dynamic features characterised by rapid changes under different conditions.

Three-dimensional tetrahedron network (3D TEN)

The 3D TEN is a 2D triangular irregular network (TIN) extension (Abdul-Rahman & Pilouk, 2007). Figure 1(a) depicts 3D TEN objects as a linked and nonoverlapping tetrahedral with six edges, four vertices and four faces. Because objects in the real world present as uneven and three-dimensional, 3D TEN may effectively represent them (Lemmon, 2010). In addition to the TIN, the 3D TEN may describe 3D objects characteristic of multifaceted spatial topological interactions and closely arrayed yet nonoverlapping tetrahedrons (Abdul-Rahman & Pilouk, 2007). The qualities of the 3D TEN data format justify its use for modelling an object with volume and rigid qualities.

Due to its high computational efficiency and well-defined groupings of triangles, easy depiction, ease of maintenance for visualisation while employing a network of quasi-tetrahedra

(Breunig et al., 2020) and adaptability in expressing complicated objects, 3D TEN was chosen as the internal data model for this study. According to (Abdul-Rahman & Pilouk, 2007), the easiest data model that can be summarised into point, line and volume depictions while creating and dividing real-world objects is 3D TEN. The capacity of 3D TEN to partition allows for the generation of models for volumes that do not overlap in a given space (Breunig et al., 2020).

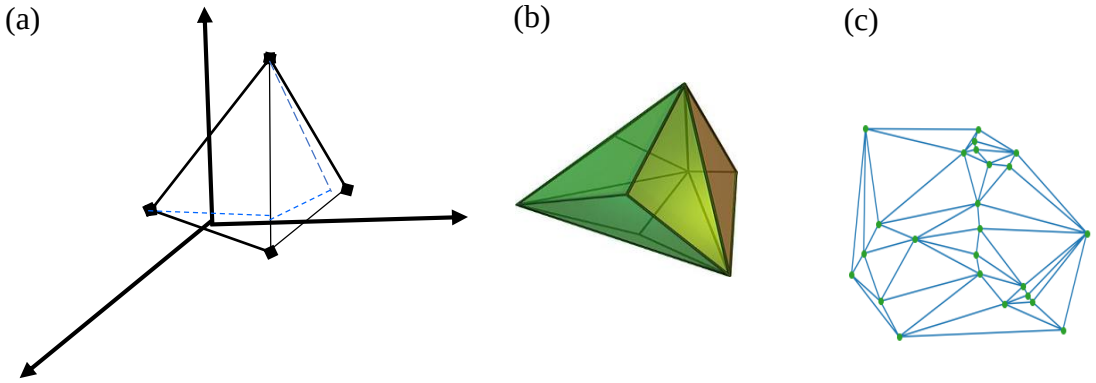

Source: modified from Ciullo et al. 2020

Figure 1. 3D TEN model and Delaunay triangulation.

Figure 1(b) shows a 3D TEN made of a tetrahedron network that allows for a 3D representation of subsurface geology based on VES interpretation. In Figure 1(c) of the resulting 3D TEN, a succession of meshes including numerous more geometric criteria relevant to interpolation accuracy are built using Delaunay triangulation. A limited Delaunay triangulation was created to reduce the Delaunay property while maintaining optimality features similar to those of a Delaunay triangulation. As a result, from the perspective of 3D modelling, the interpreted VES data may now be modelled in 3D, with groundwater movement within each of the modelled landforms simulated as a dynamic landscape.

Darcy's law-based 3D groundwater flow model

In Darcy's groundwater flow model, the flow rate is expected to be equal to the nature and features of the subsurface formation that makes up the layer in any model explaining the visualisation of groundwater flow (Langevin, 2017). This allows for groundwater flow modelling and simulation inside constrained geological features. Although current 3D data models may be used in groundwater modelling, the existing theories, processes and nature that regulate subsurface water flow must be included in 3D modelling and data visualisation to enable realist depiction.

Beni et al. (2011) established two approaches to defining alterations in the field: Eulerian methods, which allow the design in the field at a specific site using fixed points, and Lagrangian approaches, which allow the design in form, size, and volume that occur on a variable component restricted at multiple locations. A Lagrangian technique was used to depict the flow rate of water restricted in a subsurface stratum at multiple points for this study.

The 3D flow of water over different geological media was developed by implementing two techniques: water as a dynamic object that changes shape and size over varying voids of the subsurface material and flow velocity in the media determined using Darcy's law of groundwater

flow mechanism (Schwartz & Zhang, 2002) to create a unique distribution over distinct saturated formations based on Equations 1-6:

$$\frac{\partial(k_x \frac{\partial h}{\partial x})}{\partial x} + \frac{\partial(k_y \frac{\partial h}{\partial y})}{\partial y} + \frac{\partial(k_z \frac{\partial h}{\partial y}}{\partial z} = 0 \qquad (1)$$

where $\frac{\partial h}{\partial x}$,$\frac{\partial h}{\partial y}$ and $\frac{\partial h}{\partial z}$ represent fluctuations in the volume of groundwater flow along X, Y and Z, while *k represents the* permeability of the subsurface channel through which water flows. The following equation was used to enable visualisation of groundwater flow utilising the Lagrangian technique for simulation and 3D modelling of groundwater:

$$\begin{matrix} a_x & a_y & a_y \\ b_x & b_y & b_z \\ c_x & c_y & c_z \\ & \vdots & \\ n_x & n_y & n_y \end{matrix} \qquad (2)$$

In Equation 2, *a, b, c...n* represent subsurface layers, and x, y, z are measurements of the layers. In 3D Delaunay triangulation, Equation (2) depicts the anticipated function of a dynamic point. The net outflow/inflow of water in a subsurface inside a specific layer.

Materials and methods

Research framework

The research framework (Figure 2) is structured into 5 major stages: acquisition of subsurface information, delineation of the subsurface lithology, production of the layer thickness map, 3D TEN modelling of the subsurface lithology, and simulation of the groundwater using VGO over a time scale. The Niger State Geologic map was used to extract the Bida Basin Map on a scale of 1:600,000. The subsurface porosity of the geological stratum was also deduced. In addition, a groundwater potential map and a thematic layer map with distinctive geological formations were generated from the Niger state Geologic map.

To produce the subsurface thickness map of the study area, spatially referenced VES data were imported into the geodata base as Database File (.dbf). The computer iteration's demarcated layers were stored in a GIS database for geological mapping. The demarcated layer was interpolated using inverse distance weight (IDW) interpolation. The imported delineated data were then subjected to geostatistical analysis using IDW interpolation techniques, which, according to Liu *et al.* (2021) and Munyati and Sinthumule (2021), are more suitable in handling heterogeneous geological surfaces as tannable in the basin. Dynamic field simulation techniques involve the creation of a simulation of VGOs to represent water elements constrained within a 3D TEN depiction of the geological strata using 3D Studio Max software. This method was justified by the need to implement dynamic field simulation and real-time rendering in a particular location.

A 3D equation of Darcy's law of groundwater flow was adapted from a 2D field to enable groundwater simulation. Next, a single-value function of a location in a two-dimensional position

was defined as f(x,y) (Beni et al., 2011). The single-value function of a position in a 2D space was referred to as a 2D field (f). Value f (x,y,z) was generated because of the extension of a two-dimensional field into a 3D field. Upon the integration of time into the field change at a particular point within a specific geological formation, the field function became f(x(t), y(t), z(t)). As a result, Equation 3-6 then defines the instantaneous dynamics in groundwater flow in a 3D field at a particular geological layer:

$$f(a) = k\left(\frac{\frac{\partial h}{\partial x} + \frac{\partial h}{\partial y} + \frac{\partial h}{\partial z}}{\partial t}\right) = 0 \quad (3)$$

$$f(b) = k\left(\frac{\frac{\partial h}{\partial x} + \frac{\partial h}{\partial y} + \frac{\partial h}{\partial z}}{\partial t}\right) = 0 \quad (4)$$

$$f(c) = k\left(\frac{\frac{\partial h}{\partial x} + \frac{\partial h}{\partial y} + \frac{\partial h}{\partial z}}{\partial t}\right) = 0 \quad (5)$$

$$(d) = \left(\frac{\frac{\partial h}{\partial x} + \frac{\partial h}{\partial y} + \frac{\partial h}{\partial z}}{\partial t}\right) = 0 \quad (6)$$

The demarcated geological layers are a, b, c, and d. ∂x, ∂y, and ∂z are instant positions that occur in subsurface units, while ∂h represents the change in flow within a geological formation. The simulation time in hours is given by ∂t, while the porosity of the geological layer is given by *k*.

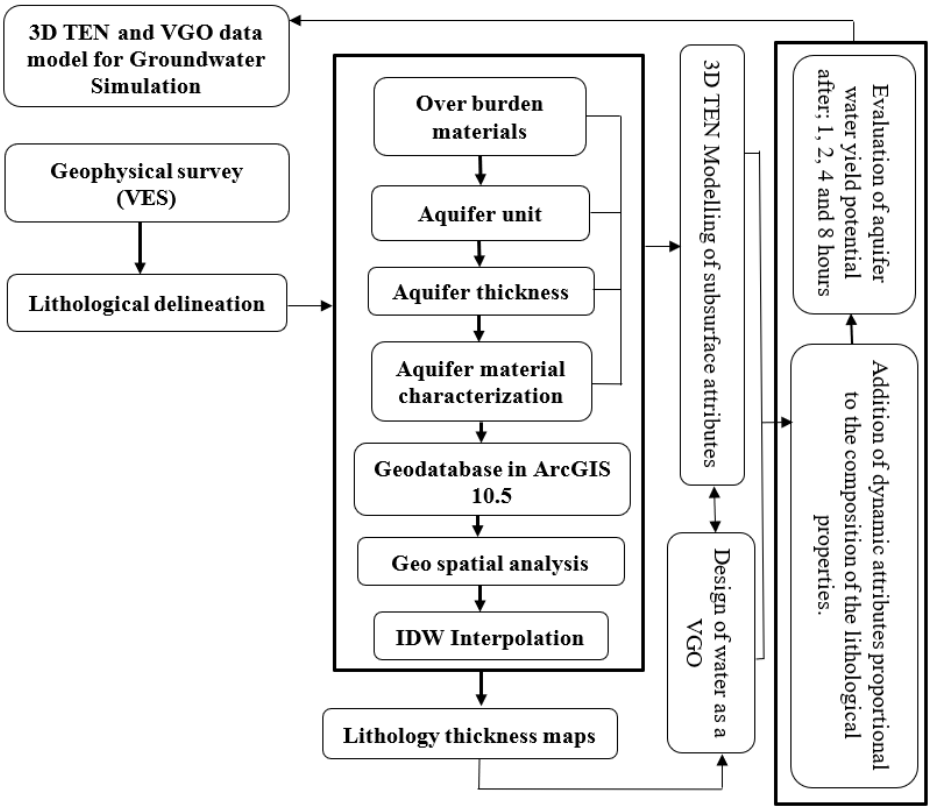

Figure 2. Research methodology flow chart

3D groundwater visualisation in VGOs

The nature, characteristics and properties of a geological layer for groundwater visualisation are largely influenced by the layer's nature, characteristics, and attributes (Binda et al., 2022). As described in Equation (6), the volume of water visualised is dependent on the nature of the overburden material, which affects the amount and quality of groundwater available for exploration around a given well (Bhattacharya et al., 2021). In addition, time is considered an important parameter in determining the borehole water recovery period, which is necessary in sustainable groundwater harvest. As with volumetric geo-objects, the water element has attributes such as shape, size, colour, speed, duration, and direction.

Water is modelled as a geo-object and is characteristic of a particle system with fundamental elements and a lifespan proportional to time. To answer the research questions of this study, water flow was simulated and designed with a mesh, as illustrated in Figure 3. The flow volume of ground water tends to rise in accordance with the particle dimensions of the geological parameters through which it flows. As time goes on and the fluid flow moves with the mesh, the mesh element locations vary constantly over time (Langevin et al., 2017).

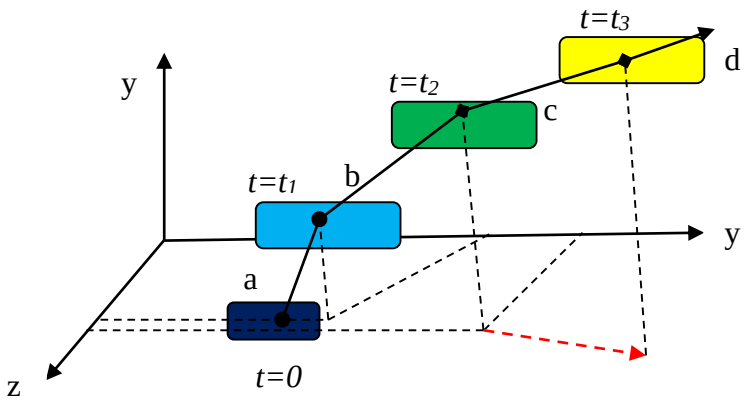

Figure 3. Simulation method implemented

Groundwater Flow Modelling and Simulation in 3D using 3D TEN and VGO

The approach used in this study for 3D modelling and groundwater simulation utilising volumetric data models and 3D TEN is as follows: (1) collecting subsurface data through the employment of VES while storing coordinates of each VES position; (2) analysing VES data through the confinement of the delimited VES strata into accessible drill records to determine the type of geology; (3) creating geographic information system maps of delimited layer width and the potential of groundwater; (4) converting the thickness of data in the Geographic Information System database to 3D using 3D TEN data arrangement; and (5) simulating groundwater flow in 3D layer modelling using VGO to depict the layer of water. The 3D Darcy's law will drive the modelled layer comprising water elements in motion. Dynamic field simulation was performed using Darcy's law and equation (Omar et al., 2020), which drive the motion of the flow field with unique speed and direction proportional to the size of the tetrahedron network mesh that represents the delineated surfaces. The Lagrangian technique was used to design the flow field within the mesh to demonstrate changes in the size and volume of the water element constrained at a sequence

of points (Izham & Rindam, 2012). Three-dimensional modelling tools and ArcGIS that are viable and accessible will be used to store the generated data.

Study area

The study area is the Bida Basin located at latitudes 6° 15' 30"E to 7° 00' 40"E and longitudes 8° 10' 00"N to 9° 31' 10"N in North Central Nigeria (Figure 4). Between longitudes, two large rivers drain the Bida Basin, namely, the Chanchaga and Gbako Rivers. Furthermore, there are also smaller channels that empty into the Niger River. This spans an area of 1.79 km^2. Geologically, the basin consists mainly of sedimentary and igneous formations with many outcrops, especially in the southeastern part of the study area between Kutigi and Enagi. Because of its significance, such as water demand, growth due to an increase in the human population, and urbanisation of adjacent populations, the basin was chosen for 3D modelling and groundwater simulation.

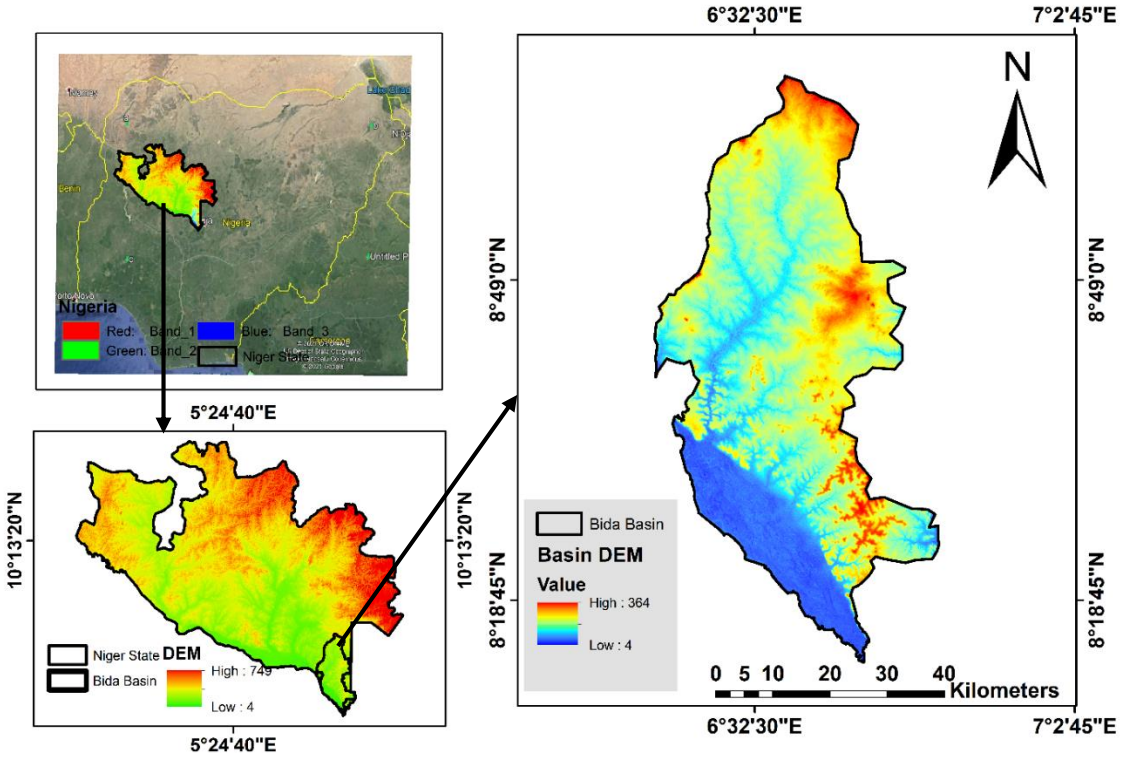

Figure 4. Location of the Bida River Basin, Northern Nigeria.

Results and discussion

Groundwater potential map and computation of layer thickness

The initial step in calculating layer thickness is to utilise the res1d.exe software, which is commercially available, and to a incorporate user-defined starting model. The resistivity survey data were used to identify the best resistivity layer and thickness (Table 1). The thickness of the identified layers alongside their geographic distribution is depicted in Figure 5. The raster grid

generated from the interpolation is placed over the 3D TEN at the same time varying the height segment to derive the 3D structure of the modelled layers. A groundwater potential map (GWP) is created (Figure 6) using the resistivity survey by applying weights to the geological formation that defined the delineated aquifer strata (Abijith et al., 2020) and estimated flow volume using Darcy's equation.

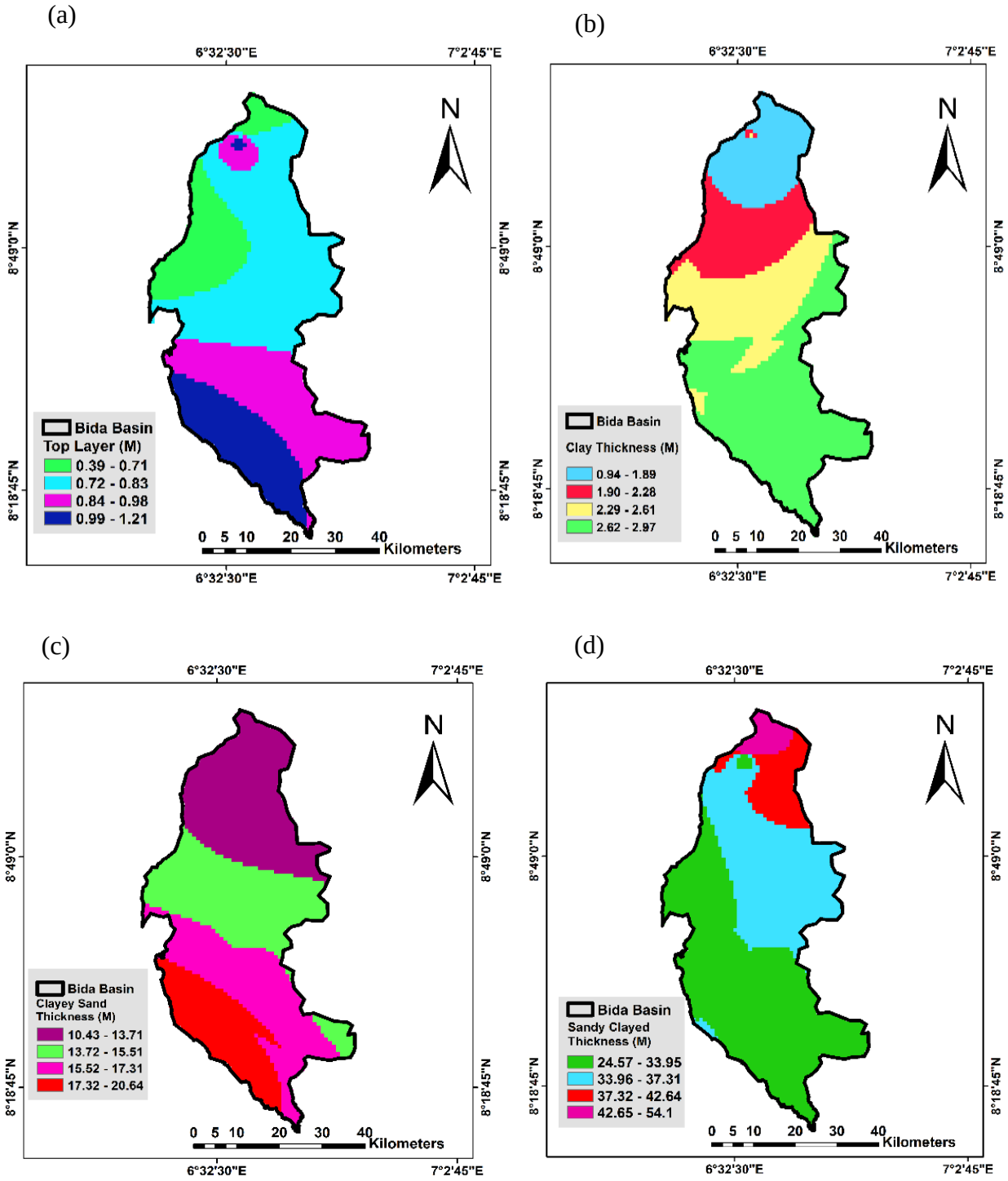

Figure 5. Subsurface layer thickness involving the (a) top layer, (b) clay, (c) clayey sand and (d) sandy clay

Table 1. Results of the resistivity survey.

VES ID	Easting	Northing	Subsurface parameters							
			LR=LAYER RESISTIVITY(Ω)				LT=LAYER THICKNESS (M)			
			LR 1	LT1	LR2	LT2	LR3	LT3	LR3	LT4
VES 1	5.47293	10.4031	1091.23	1.00	388.31	9.09	165.31	11.78	829.09	22.03
VES 2	6.73793	7.80871	1832.38	0.53	194.08	1.14	564.32	12.17	209.91	16.72
VES 3	6.30906	9.01081	1140.01	0.50	168.07	1.90	65.10	11.24	34.22	37.23
VES 4	6.31679	9.00608	1157.62	0.08	1092.29	2.34	202.54	14.79	565.58	8.45
VES 5	6.3226	9.00131	1731.93	0.05	766.42	2.41	101.66	17.56	408.19	28.35
VES 6	6.57461	9.06956	1369.39	0.36	910.21	1.44	280.63	13.66	75.92	54.73
VES 7	6.63328	9.43645	1169.16	0.40	225.84	2.25	868.44	4.18	94.29	62.44
VES 8	6.56937	9.04867	1369.04	0.81	909.92	2.44	910.21	13.66	75.91	54.73
VES 9	7.09263	8.93816	1146.92	1.00	590.70	8.59	1087.02	11.86	498.76	27.56
VES 10	6.56759	9.03734	2637.37	1.13	683.86	0.70	646.85	9.84	137.35	19.17
VES 11	5.06117	9.28963	1131.32	0.54	403.9	2.66	54.28	10.76	339.81	13.52
VES 12	5.06826	9.29931	1473.78	0.54	623.44	2.87	146.41	7.71	35.54	16.77
VES 13	5.06996	9.29434	1212.99	2.12	327.07	2.11	347.84	3.99	602.58	20.74
VES 14	5.05471	9.29434	193.87	2.17	35.01	6.49	29.96	23.02	157.31	13.30
VES 15	5.05448	9.28552	1308.77	1.56	284.03	4.16	502.51	22.17	543.55	20.30
VES 16	6.13867	9.05756	1308.39	0.52	126.50	3.75	33.18	8.69	334.34	16.95
VES 17	6.03333	9.10065	1156.37	2.55	348.24	1.32	412.45	22.87	256.32	35.00
VES 18	6.20944	8.30323	1341.26	2.45	243.65	3.74	365.56	34.89	345.50	45.89
VES 19	5.99226	9.08782	1289.68	0.67	367.07	2.67	301.34	23.89	156.67	22.56
VES 20	5.76230	8.72456	1124.32	0.54	253.11	4.50	48.28	12.84	46.78	18.45

The computed GWP map is used to identify areas with low and high groundwater volumes. The GWP map serves as a foundation for determining low and high-potential areas using 3D simulations of groundwater flow.

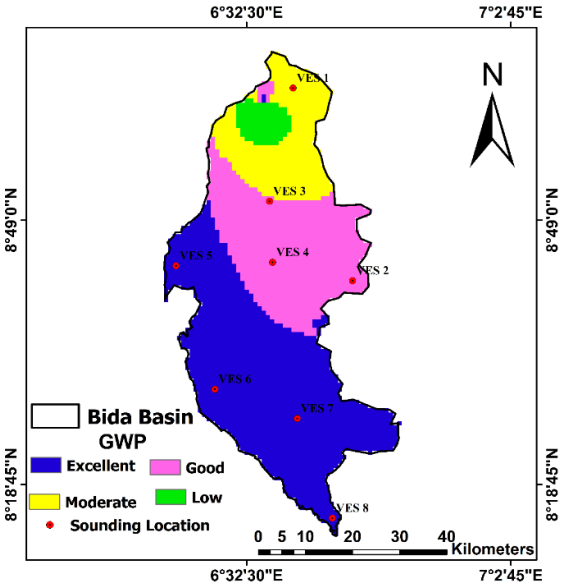

Figure 6. Bida Basin GWP map

Volumetric Geo-Object (VGO) and 3D Tetrahedron Network (3D TEN) data structures for 3D groundwater simulation

The simulated results from the VGO with the 3D TEN data model reviled distinct information withing each of the lithological units. The behaviour in the topsoil exhibits a rapid rate of movement in response to the surface topography. As the simulation time increases, the VGO objects begin to accumulate more within the relatively thinner layer compared to the thicker topsoil. This result demonstrated the high potentiality of a fast rate of infiltration of the surface soil along the low land as opposed to the relatively thicker region that might take a longer time to saturate the soil void for exploration. This, by implication, translates to high groundwater potential in the low-thickness aquifer due to a high rate of infiltration. However, such aquifers are often vulnerable to pollution and extreme weather events, such as the prevalent dry season, where the rate of recharge from both the surface and precipitation is lacking (Ahmed et al., 2021). This implication at the study area indicates a high potential of borehole failure when drilled within the first 5-10 m because of the tropical climate nature and predominantly igneous formation in some parts of the area.

VGO, which represents water in the saturated zones (Figure 7b-c), behaves in an opposite manner. VGO over the clayey zone demonstrated a low rate of saturation in the particle voids with increasing time. However, it was observed that water transmission from the layer to other layers is extremely slow despite an increase in simulation time and is thus delineated as a poor aquifer that will likely yield low groundwater for exploration. Clayey soil is generally known to have poor water transmission and percolation but has been known to yield excellent quality groundwater where it overlays and aquifers. This characteristic is due to the absence of a well interconnected network of voids for water transmission and storage during recharge. The simulation results of the sandy clay layer (Figure 7c) show an increase in the saturation rate of the VGO particles, which shows a high water retention capacity and transmission within the layer. Thus, this layer denotes the most reliable aquifer for groundwater exploration due to the high rate of infiltration and transmission exhibited by the properties of this layer. The fourth layer (Figure 7d), delineated as sandy clayey, is most confined within the very weak weather rock material. The layer is characterised by a higher depth and high saturation potential and is more likely to offer groundwater of excellent quality due to the depth, overburden material thickness, high infiltration rates and low transmissivity advantage.

Modelling resistivity data and ground surface visualisation: validation, accuracy and contribution

Based on Equations (3), (4), (5) and (6), the absolute water volume created inside the topsoil for 1 hour, 2 hours, 4 hours and 8 hours produces 17,461,228.07, 870,614.04, 435,307.02, and 348,245.61 per kilometre cube (km^3), respectively. The least water flow was observed in the clay layer due to the complexity of its pores, so the volume yield tends to be slow and low, with values recorded as follows over the same period: 330,833; 82,708.33; 41,354.17; and 33,083.33 km^3. Water volumes of 2,369.52, 29,586.91, 590,773.81, and 2,363,095.24 km^3 in the clayey sand layer indicate an increased porosity resulting from shifting from clay to sand. Due to varying sand and sandy clayey emergence, the sandy clay layer has the maximum potential water yield and potential and average flow rate, with flow volumes of 249,685.53, 312,106.91, 624,213.84 and 2,496,855.35 per km^2 respectively.

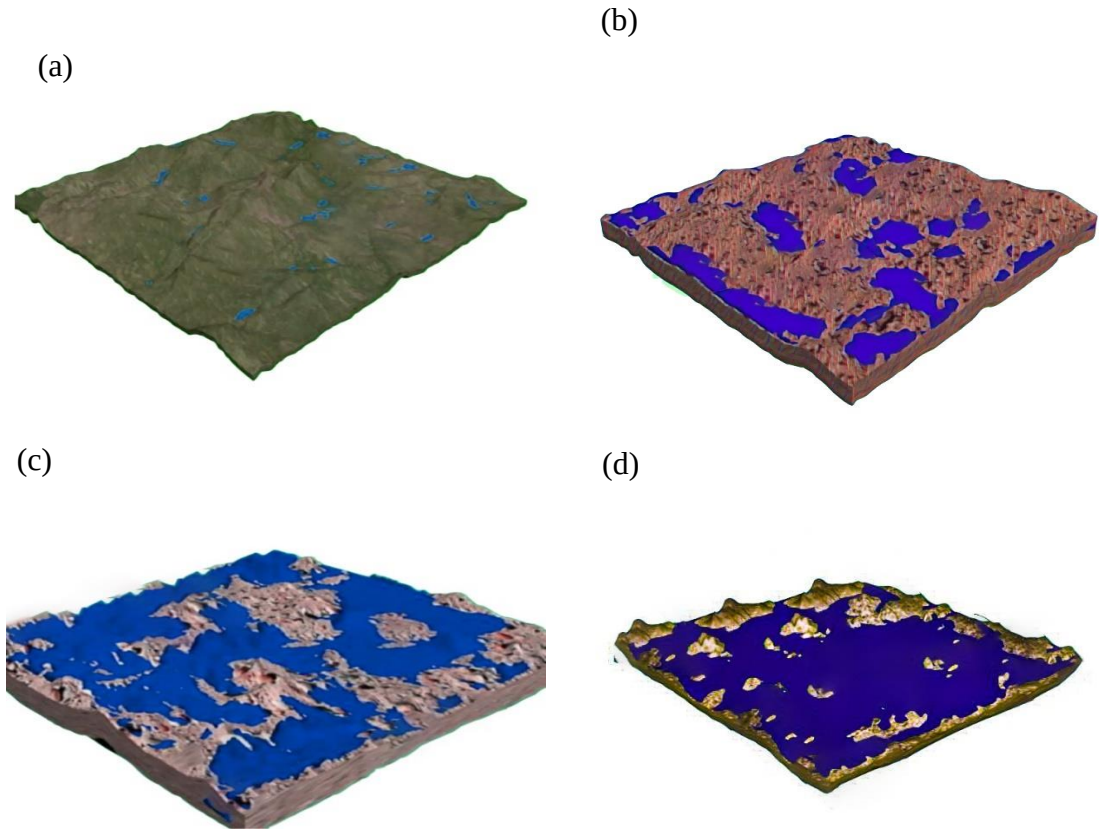

Figure 7. Three-dimensional dynamic simulation showing the combined 3D TEN and VGO data model visualised at 1 hour, 2 hours, 4 hours and 8 hours over (a) topsoil, (b) clay, (c) clay clayey sand, and (d) sandy clay

Simulations were carried out to visualise water flow at 1-hour, 2-hour, 4-hour, and 8-hour intervals due to the computed volume (i.e., resulting porosity of the subsurface layer and the geological composition). The simulation results have a significant impact on the time frame. Nevertheless, in this study, the identified prevalent geology during the ground water exploration survey was an aquifer. Despite the importance of the nature and geology of an aquifer, with regard to potential water yield, scholars such as Zaidi et al. (2017) and Abijith et al. (2020) believe that the geology of the vadose zone has an impact on the aquifer because it determines the quantity of water supplied to the aquifer via hydrogeological circulation and permeation.

The simulated result in Figure 6 continues to increase in the capacity of water (shown in blue) as the geological layer particle sizes increase. By implication, despite surface elevation, topsoils with hydrogeological movement retained very little water in response to surface slope over time. A higher water retention capacity with a corresponding low water transmission was observed in clay soil, as they possess a tighter void between its particles and low water diffusion, indicating the possibility of poor water yield potential over the clay aquitard. In comparison to the clay layer, the clay–clayey sand lithology, which contains a mix of sand and clay, appears to have a relatively high-water prospect.

Even so, clay appears to have created a spot of undulating compacted material within this layer, forming an aquitard and leaving little or no trace of water after the simulation. As a result of the large pore spaces that permit easy water movement within this layer, the sandy clay layer simulation possesses a larger volume of water compared to other geological formations, and by implication, it may result in a high water yield potential. This simulation's implications and application to groundwater investigation are as follows: the flow direction is likely to be changed in reaction to compact materials, and the nature, kind, and amount of compressed material have an impact on the potential water yield for any credible groundwater research operation.

Modelling resistivity data and ground surface visualisation: validation, accuracy and contribution

To validate and assess the modelled resistivity data along with surface visualisation, the simulated groundwater yield over time in different geological media was used to statistically evaluate the accuracy level of the implemented technique. The statistical validation will demonstrate the success rate of the 3D visualisation of groundwater flow as a VGO. The statistically validated results show a poor accuracy rate of 0.38 (38%) over the topsoil layer (Figure 8a) after an hour. In clay soil, on the other hand, the accuracy rate improves significantly to a success rate of 0.89 (89%) when the time increases to 2 hours (Figure 8b). When the time frame was doubled to 4 hours over clayey sandy soil, the accuracy of the simulated results declined slightly to a value of 0.81 (81%) (Figure 8c). Furthermore, doubling the time over sandy clayey soil maintained the same accuracy as the clayey sand layer with a value of 0.81 (81%) (Figure 8d).

Inferences into the poor accuracy over the top surface could be due to the presence of impervious surfaces of rock outcrops and clayey-like soil in many parts of the study area. Rock outcrops and clayey areas are predominantly known to have poor infiltration rates compared to the other forms of aquifers. Thus, they are often delineated as not suitable for groundwater exploration. Sandy soil has a well-established network of voids that allow for infiltration of water from the overburden material and transmission of water to the underlaying layer. This factor is likely responsible for the highest accuracy of the techniques applied in the study area. The sandy clayey and clayey sand produced the same accuracy with an increase in the simulation time rate, which was largely due to the similar behaviour of the material compositions. Although slight variation exists in the saturation rate of the layers and influence of depth, the layer produced the same accuracy indicating the aquifer marked at these formations has a high potential for producing reliable and most durable borewell the meet population demands.

However, it is critical to note that the implemented 3D TEN for the modelling of resistivity data and groundwater visualisation in a subsurface medium offers a new perspective for the 3D evaluation of groundwater prospective zones in the study area, which is an improvement over the existing VES and GIS technique that is devoid of data representation in the near real world. The developed 3D model using 3D TEN and VGO provides a new frontier in groundwater exploration research for the visualisation of subsurface layers and the behaviour of saturated zones, which are critical in the evaluation of drilling performance and reduce the high rate of borehole failure in the study area and other areas of similar geology and climate.

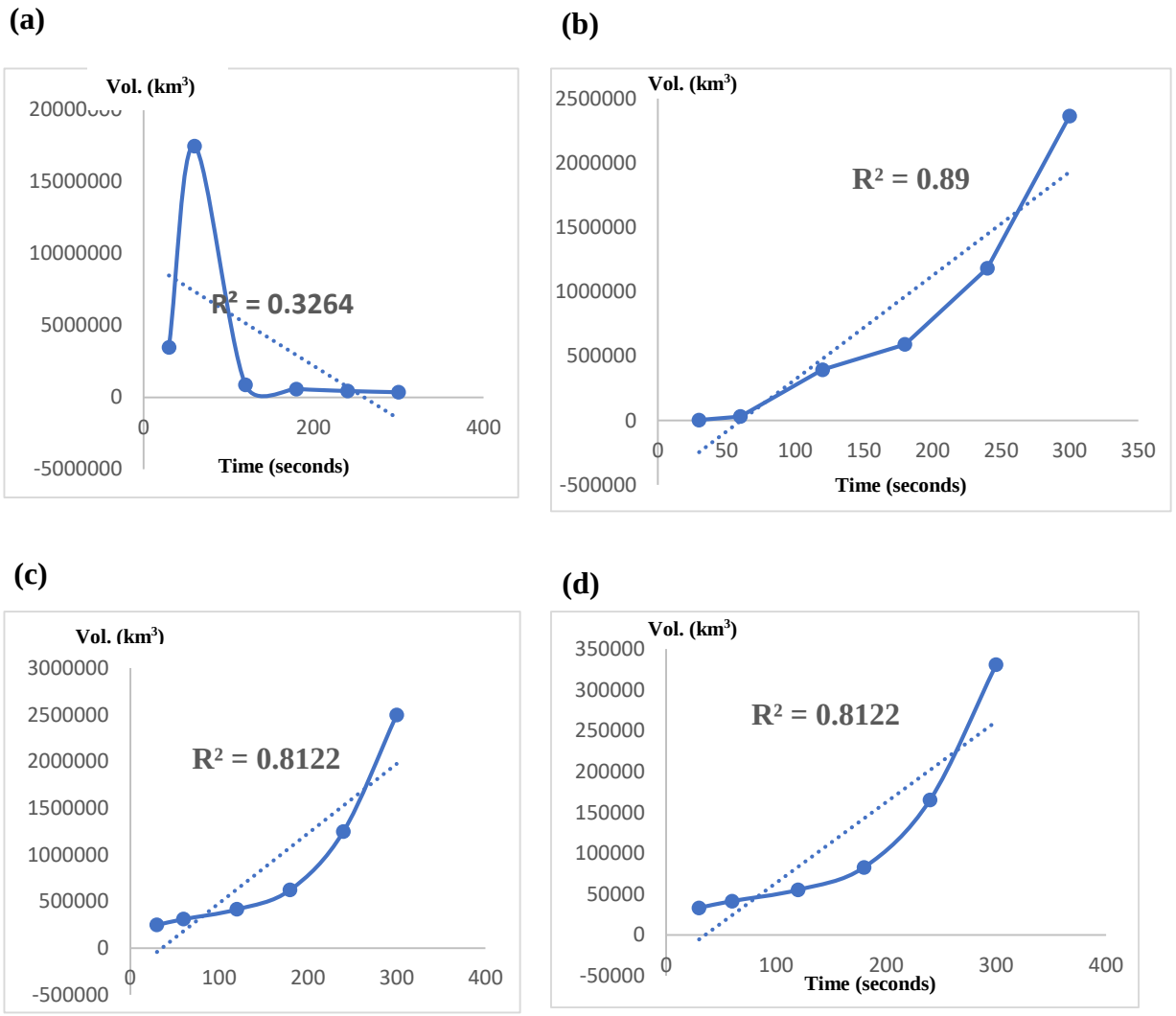

Figure 8. Accurancy assessment over (a) topsoil; (b) clay, (c) clay clayey sand; and (d) sandy clay.

Conclusions

This study utilises a 3D TEN data model in modelling VES data obtained using geophysical techniques in the Bida Basin in Nigeria to enhance the reliability of groundwater wells, which are often characterised by poor production and failure in the study area. Groundwater was then visualised and simulated within the subsurface layers using a VGO. The groundwater flow velocity and direction over the saturated zone were simulated according to Darcy's law of groundwater movement.

The results show that the VES technique was able to delineate four major aquifer layers of varying thicknesses in the study area with different water-bearing conditions that are critical for the productivity and sustainable water ned of the people. The 3D model of the VES data in 3D TEN was able to effectively model the subsurface layer in near real time. Evaluation of the simulation performance reveals reliable information about the nature, attributes and geological

composition that make up the saturated zones, which are critical for decision-making on sustainable groundwater harvesting in near real time, as opposed to the existing prospection method, which mainly focuses on the subsurface particles without recourse to the behaviour of the saturated layer behaviour, which to a large extent determines the borehole reliability. In addition, the groundwater quality, which is opaque in the existing groundwater exploration model, is adequately handled in the designed and implemented VGO within the 3D TEN mesh. Furthermore, the simulated result using VGO demonstrated that sandy clayey and clayey sand are the best saturated zones in the study area that are capable of yielding excellent groundwater that meets the community needs irrespective of the time and season of the year.

As a result, the findings of this study will be extremely useful to water practitioners and other stakeholders, such as the Ministry of Water Resources, the River Basin Development Authority, and the government, in developing policies and carrying out groundwater exploration in the basin economically.

Acknowledgement

The authors would like to sincerely appreciate the two anonymous reviewers for their constructive critiques towards improving the quality of the manuscript.

References

Abdul-Rahman, A., & Pilouk, M. (2007). *Spatial data modelling for 3D GIS*. New York, Springer Berlin Heidelberg

Abijith, D., Saravanan, S., Singh, L., Jennifer, J. J., Saranya, T., & Parthasarathy, K. S. S. (2020). GIS-based multi-criteria analysis for identification of potential groundwater recharge zones - a case study from Ponnaniyaru watershed, Tamil Nadu, India. *HydroResearch, 3*, 1-14. doi:https://doi.org/10.1016/j.hydres.2020.02.002

Ahmad, I., Khan, M. N., Inc, M., Ahmad, H., & Nisar, K. S. (2020). Numerical simulation of simulate an anomalous solute transport model via local meshless method. *Alexandria Engineering Journal, 59*(4), 2827-2838. doi:https://doi.org/10.1016/j.aej.2020.06.029

Ahmed, A., Alrajhi, A., & Alquwaizany, A. S. (2021). Identification of Groundwater Potential Recharge Zones in Flinders Ranges, South Australia Using Remote Sensing, GIS, and MIF Techniques. *Water, 13*(18), 2571.

Akinyemi, O. D. (2022). Multivariate interrelatedness of geotechnical and petrophysical properties towards developing near-surface lithology clusters in a sedimentary terrain. *Bulletin of Engineering Geology and the Environment, 81*(7), 258. doi:10.1007/s10064-022-02755-3

Andriani, G. F., Pastore, N., Giasi, C. I., & Parise, M. (2021). Hydraulic properties of unsaturated calcarenites by means of a new integrated approach. *Journal of Hydrology, 602*, 126730. doi:https://doi.org/10.1016/j.jhydrol.2021.126730

Anh, N. G. T. (2011). Overview of Three-Dimensional GIS Data Models. Paper presented at the International Conference on Technological Advancements in Civil Engineering ICTACE India- Chennai, India-Chennai.

Arowoogun, K. I., & Osinowo, O. O. (2022). 3D resistivity model of 1D vertical electrical sounding (VES) data for groundwater potential and aquifer protective capacity assessment:

a case study. *Modeling Earth Systems and Environment, 8*(2), 2615-2626. doi:10.1007/s40808-021-01254-w

Beni, H., Leila Mostafavi, Mir Abolfazl Pouliot, & Jacynthe Gavrilova, M. (2011). Toward 3D spatial dynamic field simulation within GIS using kinetic Voronoi diagram and Delaunay tetrahedralization. *International Journal of Geographical Information Science, 25*(1), 25-50. doi:https://doi.org/10.1080/13658811003601430

Bhattacharya, S., Das, S., Das, S., Kalashetty, M., & Warghat, S. R. (2021). An integrated approach for mapping groundwater potential applying geospatial and MIF techniques in the semiarid region. *Environment, Development and Sustainability, 23*(1), 495-510.

Binda, G., Frascoli, F., Spanu, D., Ferrario, M. F., Terrana, S., Gambillara, R., Trotta, S., Noble, P. J., Livio, F. A., Pozzi, A., & Michetti, A. M. (2022). Geochemical Markers as a Tool for the Characterization of a Multi-Layer Urban Aquifer: The Case Study of Como (Northern Italy). *Water, 14*(1), 124. doi: https://doi.org/10.3390/w14010124

Breunig, M., Bradley, P. E., Jahn, M., Kuper, P., Mazroob, N., Rösch, N., Al-Doori, M., Stefanakis, E., & Jadidi, M. (2020). Geospatial Data Management Research: Progress and Future Directions. *ISPRS International Journal of Geo-Information, 9*(2), 95.

Cedrick, M. M., Alexander, A., Nobert, J., & Mbudi, C. N. U. D. (2021). Modeling groundwater flow under chaotic urbanization constraints in Kinshasa Capital Region (D.R. Congo). *Physics and Chemistry of the Earth, Parts A/B/C, 124*, 102985. doi:https://doi.org/10.1016/j.pce.2021.102985

Ciullo, V., Rossi, L., & Pieri, A. (2020). Experimental Fire Measurement with UAV Multimodal Stereovision. *Remote Sensing, 12*(21), 3546.

Di Salvo, C., Mancini, M., Cavinato, G. P., Moscatelli, M., Simionato, M., Stigliano, F., Rea, R., & Rodi, A. (2020). A 3D Geological Model as a Base for the Development of a Conceptual Groundwater Scheme in the Area of the Colosseum (Rome, Italy). *Geosciences, 10*(7), 266.

Ekanem, A. M. (2020). Georesistivity modelling and appraisal of soil water retention capacity in Akwa Ibom State University main campus and its environs, Southern Nigeria. *Modeling Earth Systems and Environment, 6*(4), 2597-2608. doi:10.1007/s40808-020-00850-6

Fanos, A. M., Pradhan, B., Alamri, A., & Lee, C.-W. (2020). Machine learning-based and 3d kinematic models for rockfall hazard assessment using LiDAR data and GIS. *Remote Sensing, 12*(11), 1755.

Gaikwad, S., Pawar, N. J., Bedse, P., Wagh, V., & Kadam, A. (2022). Delineation of groundwater potential zones using vertical electrical sounding (VES) in a complex bedrock geological setting of the West Coast of India. *Modeling Earth Systems and Environment, 8*(2), 2233-2247. doi:10.1007/s40808-021-01223-3

Gong, J.Y., Cheng, P.G. & Wang, Y. D. (2004). Three-dimensional modelling and application in geological exploration engineering. *Computers & Geosciences*, *30*, 391–404.

Havenith, H.-B. (2021). 3D Landslide Models in VR. In B. Tiwari, K. Sassa, P. T. Bobrowsky, & K. Takara (Eds.), *Understanding and Reducing Landslide Disaster Risk: Volume 4 Testing, Modeling and Risk Assessment* (pp. 195-204). Cham: Springer International Publishing.

Huang, X., Li, H., Li, X., & Zhang, L. (2019). *Fire numerical simulation analysis for large-scale public building in 3D GIS.* Paper presented at the IGARSS 2019 - 2019 IEEE International Geoscience and Remote Sensing Symposium.

Izham, M. Y., Uznir, U. M., Alias, A. R., Ayob, K., & Ruslan, I. W. (2011). Influence of georeference for saturated excess overland flow modelling using 3D volumetric soft geo-objects. *Computers & geosciences, 37*(4), 598-609. doi:10.1016/j.cageo.2010.05.013

Izham, Y. M., & Rindam, M. (2012). 3D GIS urban runoff mechanism: A new perspective using volumetric soft geo-object. *Geografia: Malaysia Journal of Society and Space 8*(5), 124-139.

Jaxa-Rozen, M., Kwakkel, J. H., & Bloemendal, M. (2019). A coupled simulation architecture for agent-based/geohydrological modelling with NetLogo and MODFLOW. *Environmental Modelling & Software, 115*, 19-37. doi:https://doi.org/10.1016/j.envsoft.2019.01.020

Joy, J., Kanga, S., & Singh, S. K. (2020). 3D GIS retrospective flood visualisation. *Acta. Tech. Corvin. Bull. Eng, 13*(2), 13-18.

Lamontagne-Hallé, P., McKenzie, J. M., Kurylyk, B. L., Molson, J., & Lyon, L. N. (2020). Guidelines for cold-regions groundwater numerical modeling. *Wiley Interdisciplinary Reviews: Water, 7*(6), e1467. doi: 10.1002/wat2.1467

Langevin, C.D., Hughes, J.D., Provost, A.M., Banta, E.R., Niswonger, R.G., Panday, S. (2017). Documentation for the MODFLOW 6 Groundwater Flow (GWF) Model. *U.S. Geological Survey Techniques and Methods, Book 6, A55*, 197, 10.3133/tm6A55.

Lemmon, C. J. (2010). *Boundary mapping and its application to geographic routing* (PhD dissertation). Retrieved from James Cook University.

Li, L., Xia, F., Liu, J., Zang, K., Liu, C., Wei, J., & Liu, L. (2022). 3D Quantitative Prediction of the Groundwater Potential Area─A Case Study of a Simple Geological Structure Aquifer. *ACS Omega, 7*(21), 18004-18016. doi:10.1021/acsomega.2c01387

Li, W., Zhu, J., Fu, L., Zhu, Q., Xie, Y., & Hu, Y. (2021). An augmented representation method of debris flow scenes to improve public perception. *International Journal of Geographical Information Science, 35*(8), 1521-1544. doi:10.1080/13658816.2020.1833016

Li, X., Ke, T., Wang, Y., Zhou, T., Li, D., Tong, F., & Wen, J. (2020). Hydraulic conductivity behaviors of karst aquifer with conduit-fissure geomaterials. *Frontiers in Earth Science, 8*, 30.

Liu, Z., Zhang, Z., Zhou, C., Ming, W., & Du, Z. (2021). An Adaptive Inverse-Distance Weighting Interpolation Method Considering Spatial Differentiation in 3D Geological Modeling. *Geosciences, 11*(2), 51.

Luo, P., Luo, M., Li, F., Qi, X., Huo, A., Wang, Z., He, B., Takara, K., Nover, D., & Wang, Y. (2022). Urban flood numerical simulation: Research, methods and future perspectives. *Environmental Modelling & Software, 156*, 105478. doi:https://doi.org/10.1016/j.envsoft.2022.105478

Maiti, A., & Chakravarty, D. (2021). 3D reconstruction–based numerical modeling of irregular-shaped geo-objects using digital images: a novel approach. *Bulletin of Engineering Geology and the Environment, 80*(8), 6145-6160. doi:10.1007/s10064-021-02322-2

Morosini, R., Zucaro, F. (2019). Land use and urban sustainability assessment: A 3D GIS application to a case study in Gozo. *City Territ Architecture, 6*(7), https://doi.org/10.1186/s40410-019-0106-z.

Munyati, C., & Sinthumule, N. I. (2021). Comparative suitability of ordinary kriging and Inverse Distance Weighted interpolation for indicating intactness gradients on threatened savannah woodland and forest stands. *Environmental and Sustainability Indicators, 12*, 100151. doi:https://doi.org/10.1016/j.indic.2021.100151

Nasir, A. A. M., Azri, S., & Ujang, U. (2021). Modelling immovable asset in 3d using citygml 3.0 concept to support smart city initiatives. *Int. Arch. Photogramm. Remote Sens. Spatial Inf. Sci., XLVI-4/W5-2021*, 391-396. doi:10.5194/isprs-archives-XLVI-4-W5-2021-391-2021

Omar, P. J., Gaur, S., Dwivedi, S., & Dikshit, P. (2020). A modular three-dimensional scenario-based numerical modelling of groundwater flow. *Water Resources Management, 34*(6), 1913-1932. doi:https://doi.org/10.1007/s11269-020-02538-z

Omolaiye, G. E., Oladapo, I. M., Ayolabi, A. E., Akinwale, R. P., Akinola, A. A., Omolaye, K. L., & Sanuade, O. A. (2020). Integration of remote sensing, GIS and 2D resistivity methods in groundwater development. *Applied Water Science, 10*(6), 129. doi:10.1007/s13201-020-01219-x

Rydvanskiy, R., & Hedley, N. (2020). 3d geovisualization interfaces as flood risk management platforms: capability, potential, and implications for practice. *Cartographica: The International Journal for Geographic Information and Geovisualization, 55*(4), 281-290.

Schwartz, F. W., & Zhang, H. (2002). Basic Principle of Groundwater Flow. In R. Flahive, D. Powell, & N. M. Pigliucci (Eds.), *Fundamentals of ground water* (pp. 42-65): John Wiley & Sons.

Tuan, A. N. G. (2013). Overview of three-dimensional GIS data models. *International Journal of Future Computer and Communication, 2*(3), 270.

Webb, J.R., Santos, I.R., Maher, D.T., Tait, D.R., Cyronak, T., Sadat-Noori, M., Macklin, P., Jeffrey, L.C. (2019). Groundwater as a source of dissolved organic matter to coastal waters: Insights from radon and CDOM observations in 12 shallow coastal systems. *Limnology and Oceanography, 64*(1), 182-196.

Xiang, Z., Bailey, R. T., Nozari, S., Husain, Z., Kisekka, I., Sharda, V., & Gowda, P. (2020). DSSAT-MODFLOW: A new modeling framework for exploring groundwater conservation strategies in irrigated areas. *Agricultural Water Management, 232*, 106033. doi:https://doi.org/10.1016/j.agwat.2020.106033

Xu, S. (2021). Three-Dimensional Visualization Algorithm Simulation of Construction Management Based on GIS and VR Technology. *Complexity*. doi:https://doi.org/10.1155/2021/6631999.

Zaidi, S. M., Akbari, A., Abu Samah, A., Kong, N. S., Gisen, A., & Isabella, J. (2017). Landsat-5 Time Series Analysis for Land Use/Land Cover Change Detection Using NDVI and Semi-Supervised Classification Techniques. *Polish Journal of Environmental Studies, 26*(6).

Zang, F. (2022). *Application of 3D Geological Modeling in Geological Exploration.* Paper presented at the Frontier Computing, Singapore.

Zavari, M., Shahhosseini, V., Ardeshir, A., & Sebt, M. H. (2022). Multi-objective optimization of dynamic construction site layout using BIM and GIS. *Journal of Building Engineering, 52*, 104518. doi:https://doi.org/10.1016/j.jobe.2022.104518

Zeitoun, R., Vandergeest, M., Vasava, H. B., Machado, P. V. F., Jordan, S., Parkin, G., Wagner-Riddle, C., & Biswas, A. (2021). In-Situ Estimation of Soil Water Retention Curve in Silt Loam and Loamy Sand Soils at Different Soil Depths. *Sensors, 21*(2), 447.